Machining of Aluminium with MHz High-Intensity Focused Ultrasound

Pudas, Topi Matias

IEEE
2022-12-01

Pudas , T M , Hyvönen , J T J , Holmström , A , Sillanpää , T O N , Lassila , P J , Mäkinen , J M K , Kuronen , A , Kotiaho , T , Salmi , A & Haeggström , E 2022 , Machining of Aluminium with MHz High-Intensity Focused Ultrasound . in 2022 IEEE International Ultrasonics Symposium (IUS) . IEEE , pp. 1-4 , 2022 IEEE International Ultrasonics Symposium (IUS) , Venice , Italy , 10/10/2022 . https://doi.org/10.1109/IUS54386.2022.9957698

http://hdl.handle.net/10138/355159
https://doi.org/10.1109/IUS54386.2022.9957698

submittedVersion

Machining of Aluminium with MHz High-Intensity Focused Ultrasound

Topi Pudas
Electronics Research Lab., University of Helsinki
Helsinki, Finland
topi.pudas@helsinki.fi

Jere Hyvönen
Electronics Research Lab., University of Helsinki
Helsinki, Finland
jere.hyvonen@helsinki.fi

Axi Holmström
Electronics Research Lab., University of Helsinki
Helsinki, Finland
axi.holmstrom@helsinki.fi

Tom Sillanpää
Electronics Research Lab. and Faculty of Pharmacy, University of Helsinki
Helsinki, Finland
tom.sillanpaa@helsinki.fi

Petri Lassila
Electronics Research Lab., University of Helsinki
Helsinki, Finland
petri.j.lassila@helsinki.fi

Joni Mäkinen
Electronics Research Lab., University of Helsinki
Helsinki, Finland
joni.mk.makinen@helsinki.fi

Antti Kuronen
Department of Physics, University of Helsinki
Helsinki, Finland
antti.kuronen@helsinki.fi

Tapio Kotiaho
Faculty of Pharmacy and Department of Chemistry, University of Helsinki
Helsinki, Finland
tapio.kotiaho@helsinki.fi

Ari Salmi
Electronics Research Lab. University of Helsinki
Helsinki, Finland
ari.salmi@helsinki.fi

Edward Hæggström
Electronics Research Lab., University of Helsinki
Helsinki, Finland
edward.haeggstrom@helsinki.fi

***Abstract*—Cavitation-induced surface erosion has been studied for decades. High-intensity focused ultrasound (HIFU) enables localized erosion, with applications in many fields. However, no research has been published on machining solely with HIFU. Compared to existing micro-machining technologies, HIFU exhibits a unique set of benefits: inexpensive, minimal maintenance due to non-contact machining without slurry, mitigated chemical load, and monitoring capability. We demonstrate controlled surface machining of mirror-polished aluminium (AW-5754) using high-frequency (12 MHz) HIFU-induced cavitation erosion. Optimal sonication parameters (transducer-sample distance, amplitude, cycles per burst, number of bursts, and pulse repetition frequency) for stationary surface erosion were first identified experimentally. These parameters served as a basis for studying the effect of sonication parameters during on-the-fly erosion, i.e., engraving lines. The effect of stage translation velocity and the number of repeated passes across the engraved line were also studied. Subsequently, the acronym of our laboratory, "ETLA", was engraved, with a 500 µm letter height and an average line width of 53 µm.**

Keywords— Micromachining, cavitation erosion, MHz high-intensity focused ultrasound

I. Introduction

Micrometer-scale machining has become an essential tool in many fields, e.g. medicine, biotechnology, electronics, and optics. Notable applications include drug delivery systems, chemical microreactors, and micro-electromechanical systems [1, 2, 3]. Various micrometer-scale machining technologies have been developed over the past decades, each with its own benefits and limitations.

Micro-cutting involves material removal by the mechanical grinding of a tool against a workpiece [4]. A related mechanical approach is ultrasonic machining, involving surface erosion by grinding a slurry of abrasive particles with a sonotrode against a workpiece surface [5]. Micro-electro-discharge machining removes material via an electric spark discharge between an oppositely charged tool and workpiece in liquid dielectric immersion [4]. Laser micro-machining uses high-power lasers to vaporize material from the workpiece, although prolonged treatment can risk thermal damage (e.g. microcracks, recast layers) to the workpiece [4]. Focused ion-beam milling employs a beam of high velocity ions to cause erosion [4]. Etching lithography utilizes a sequence of chemical treatments and light exposure to produce patterned surfaces [3]. Mechanical machining technologies, while relatively inexpensive, require tool maintenance due to wear [6]. Laser and ion-beam milling can produce µm and nm-scale features, respectively, but are expensive relative to alternative technologies. Etching lithography can also create nm-scale features, but it requires a chemically compatible workpiece material and involves multi-stage chemical processing.

Acoustic cavitation is a phenomenon where pressure waves cause the formation and oscillation of bubbles in liquids. Once the quantity and concentration of oscillating bubbles surpasses a critical point, bubbles form unstable gas clouds (cloud cavitation) [7]. With sufficient negative pressure amplitudes, the formed bubbles can collapse at speeds approaching the speed of sound in the liquid (inertial cavitation) [8]. In the proximity of a solid surface, the inertial collapse of a single bubble can result in an inrush of liquid towards the surface, i.e. microjetting (Fig. 1).

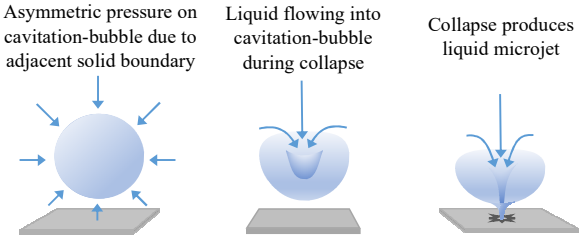

Fig. 1. Evolution of cavitation-bubble collapse near solid surface.

This work was funded by the Academy of Finland (grant 349200).

The microjet imparts a water hammer pressure on the surface. Successive collapses with sufficient water hammer pressures can cause material fatigue, resulting in localized erosion [9]. An increase in the magnitude of the acoustic rarefaction pressure (up to saturation) can therefore be expected to reduce the number of acoustic pulses required to initiate surface erosion. In practice, cavitation erosion is caused by mechanisms associated with the collective collapse of adjacent bubbles (cloud collapse). In addition to microjet impact, secondary rebound bubble implosion (the formation and subsequent collapse of bubbles generated from the primary collapse) and intermediate radical oxides (water-derived volatile gasses formed due to the high local pressures and temperatures) can play a significant role in producing erosion [10, 11].

High-intensity focused ultrasound (HIFU)-induced cavitation has been applied as a localized ablation method in a range of medical treatments, including non-invasive erosion of hard materials (lithotripsy), e.g. kidney stones [12], and soft tissues (histotripsy), e.g. scarring heart tissue to mitigate irregular electrical signals [13]. Non-focused ultrasound-induced cavitation has been widely researched as a means of surface modification, e.g. surface roughening and nanofoam formation [14, 11]. Rather surprisingly, no research has been published on machining solely with HIFU. HIFU-induced cavitation machining would introduce a unique set of benefits compared to existing machining technologies: inexpensive, minimal maintenance due to non-contact machining without slurry, mitigated chemical load due to water immersion operation, and feasibility for thermally sensitive materials.

Here we demonstrate controlled surface machining of aluminium (AW-5754) using high-frequency (12 MHz; 125 µm wavelength in water) with HIFU-induced cavitation erosion. The effect of sonication parameters on engraving linewidth, depth and line uniformity were studied. Finally, the acronym of our research laboratory, "ETLA", was engraved. Engraved features were quantified with a coded-excitation scanning acoustic microscope (CESAM) [15].

II. Methods

A. Experimental Setup

Fig. 2 illustrates the experimental setup. A custom-built transducer was prepared by epoxying (bisphenol-A/epichlorohydrin-based epoxy) a piezo bowl (f_c = 12 MHz, Ø = 1.9 cm, focal distance = 1.5 cm) to a 3D-printed support. The sonication target was an aluminium (AW-5754) plate, placed in a container filled with 400 ml of water. A mirror surface was prepared on the aluminium plate using a grinder-polisher (TegraPol-25, Stuers, Copenhagen, Denmark) with polishing paste (Aka-mono+, monocrystalline diamond suspensions, 15 µm & 6 µm). To control the concentration of contaminants and dissolved gas, the water was purified with a purification system (RiOs Essential Water Purification Systems, Milli-Q, Hesse, Germany) and kept in vacuum for 20 min.

The 12 MHz focused transducer was mounted onto a 3-axis motorized linear translation stage (NLS4 NEMA 17 MDrive, Newmark Systems Inc., California, USA). Actuation signals were produced with a waveform generator (AFG31052 SERIES, Tektronix, Oregon, USA). The actuating signal was amplified using an RF amplifier

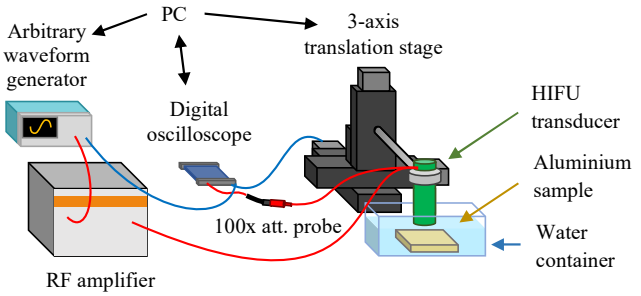

Fig. 2. Experimental setup. A HIFU transducer, mounted onto a 3-axis translation stage, is lowered into a water-filled container with the aluminium sample. Amplified signals are delivered from a waveform generator to the transducer. A digital oscilloscope monitors the signal received by the transducer and acoustic echoes returning from the aluminium surface. Signal triggers for both actuation and monitoring are delivered by PC via the translation stage. Red lines indicate actuation signal paths, blue lines trigger signal paths.

(500A100A, Amplifier Research, Pennsylvania, USA). A 100x attenuation probe (TT-HV250, TESTEC Elektronik GmbH, Hesse, Germany) was used with a digital oscilloscope (Picoscope 5442D, Pico Technology, Cambridgeshire, UK) to record the amplified signal for conversion to pressure values. Triggers to the waveform generator, oscilloscope and translation stages were provided by PC (via the translation stages).

B. Pressure Calibration

Conversion of measured voltage values produced by the amplifier to acoustic pressure values was based on calibration measurements. Pressure values were measured with a needle hydrophone (Ø = 75 µm, Precision Acoustics Ltd., Dorchester, UK) at the focal point at low amplitudes (< 90 V), and 1 mm from the focal point along the optical axis of the transducer at high (> 140 V) and low amplitudes. Based on the linear trend across high and low amplitudes in recorded off-focus pressures, a linear function for extrapolating focal amplitude values for high excitation voltages was used to convert excitation voltages to peak-positive-pressures.

C. Sonication Parameter Study

Preliminary experiments were carried out to identify optimal sonication parameters for producing erosion at stationary sites. The resultant parameters were: transducer-sample distance of 15.24 mm, peak-positive-pressure amplitudes of ~30 MPa, 50 cycles per burst, 10 000 bursts. Continuing from stationary sonication to sonication on-the-move (engraving), parameters were varied around these values.

Engraving was done by performing repeated passes over the target while sonicating. While keeping the total input energy constant, the effect of movement velocity, number of passes, pulse repetition frequency (PRF) and cycles per burst was studied. Two velocities of 50 µm/s and 500 µm/s were used to engrave 1 mm long lines, the first with 20 passes and the latter with 200 passes. PRF and burst cycles were varied together: 250 Hz and 100 cycles, 500 Hz and 50 cycles, 1 kHz and 25 cycles.

Next the effect of total input energy was studied by altering acoustic amplitude, cycles per burst, and the number of passes. Velocity and PRF were kept constant at 50 µm/s

and 250 Hz. Peak-positive-pressure amplitudes were 26 MPa, 33 MPa, and 38 MPa. For each amplitude value, 9 engravings were performed with varying cycles per burst and passes: 50, 100, and 200 cycles, and 10, 20, and 30 passes.

Based on these experiments, 33 MPa, 200 cycles, 250 Hz PRF and 20 passes were selected to engrave the text "ETLA". The letters were 500 µm long, with 125 µm spacing between letters.

D. Coded-Excitation Scanning Acoustic Microscope

The cavitation erosion of sonicated samples was imaged with a CESAM [15]. Measured surface topography maps enabled quantification of erosion depth and surface area profiles. The specific configuration and principles of operation of the microscope have been outlined by Hyvönen *et al.* [16] and Meriläinen *et al.* [15].

III. Results and Discussion

A SAM topography map of 1 mm long engraved lines produced with varying sonication parameters, while maintaining constant total energy input, is presented in Fig. 3. Lines produced with 20 passes at 50 µm/s translation velocity are slightly thicker than those produced with 200 passes at 500 µm/s (in order of increasing cycles: 51 µm vs. 45 µm, 51 µm vs. 45 µm, 53 µm vs. 50 µm). In contrast, the relative standard deviation of line width tends to be greater for lines produced with 200 passes (0.28 vs. 0.29, 0.27 vs. 0.35, 0.27 vs. 0.37). These slight variations could be attributed to differences in the spatial separation between consecutive acoustic pulses. At 50 µm/s and 250 Hz PRF the spatial separation between acoustic pulses along the engraved line is 200 nm, while at 500 µm/s and 250 Hz PRF the corresponding separation is 20 µm. Using standard equations from optics, the theoretical focal beam diameter (at full-width-half-maximum) of our transducer is 140 µm [17]. Evidently, a 20 µm spatial separation between acoustic pulses is significant relative to the focal beam diameter, while a 200 nm movement comprises virtually stationary sonications. Since the cavitation cloud is confined within the focal beam, a smaller translational step between consecutive sonications can be expected to improve the symmetry of bubble distribution within the subsequent cavitation cloud.

SAM topography maps of 1 mm long engraved lines produced with constant velocity and PRF, and varying amplitudes, cycles per burst and number of passes are shown in Fig. 4. A similar trend can be seen for all varied parameters: Increasing amplitude, cycles per burst or passes produces wider lines. This is to be expected, since all three parameters are proportional to the total acoustic energy input. All lines display a degree of nonuniformity, which can be attributed to the stochasticity of cloud cavitation caused by variations in environmental conditions, e.g., the number of bubbles, bubble distribution, and surface irregularities acting as bubble nucleation sites. All lines engraved with 50 cycles (top rows) display some degree of segmentation, excluding 33 MPa, 30 passes. This segmentation suggests that 50 cycles is insufficient to reliably onset inertial cavitation at the used amplitudes, i.e., the effective cavitation probability is inadequate for consistent engraving.

Evidently the most consistent erosion is produced with the highest amplitude. While a higher amplitude increases cavitation probability, it also causes a larger portion of the transducer focal zone to surpass the cavitation threshold pressure. To allow for sufficiently high cavitation probability with minimal expansion of the active focal zone, 33 MPa, 200 cycles and 20 passes were selected as the sonication parameters for subsequent engraving. The average line width and depth of the corresponding line in Fig. 4 were (43 ± 13) µm and (20 ± 8) µm, respectively, where uncertainties are standard deviations. Peripheral surface roughening was present around each engraved line (not visible in the SAM images due to color axis window), which can be attributed to infrequent cavitation events induced in the side lobes of the focal beam, and microjet-induced rebound cavitation events [18]. Intermediate gaseous radicals formed during cavitation also participate in the erosion of oxidizable metals by forming unstable oxides [19, 11]. However, the magnitude of this effect in comparison to microjets, i.e., the interplay of chemical and physical erosion mechanisms, is poorly understood in literature.

A SAM topography map of engraved letters "ETLA" is presented in Fig. 5. The average line width and depth were (53 ± 22) µm (corresponding to 0.42 λ) and (23 ± 10) µm, respectively, where uncertainties are expressed as standard deviations. Line width appears to increase near the

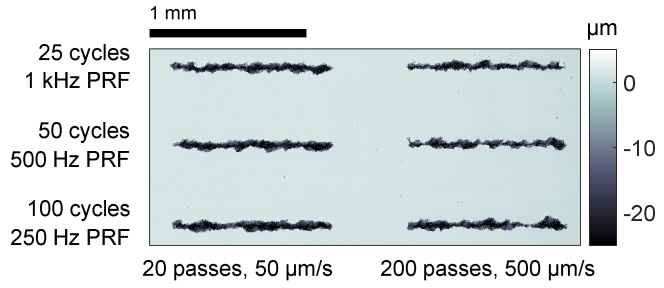

Fig. 3. SAM surface topography map of lines engraved on aluminium with 12 MHz HIFU-induced cavitation. A positive acoustic amplitude of 33 MPa was kept constant. Other sonication parameters were varied to maintain constant total energy input.

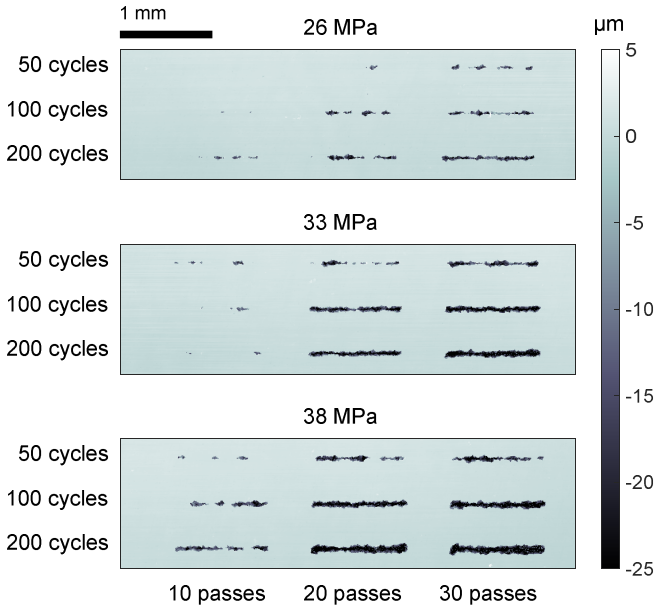

Fig. 4. SAM surface topography maps of lines engraved on aluminium with 12 MHz HIFU-induced cavitation. Translational velocity and PRF were kept constant at 50 µm/s and 250 Hz. Acoustic peak-positive-pressure, cycles per burst and number of repeated passes were varied.

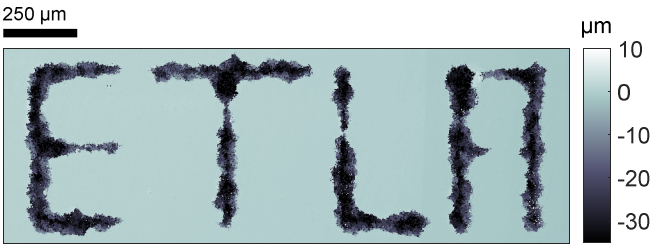

Fig. 5. SAM surface topography map of text “ETLA” engraved on aluminium with 12 MHz HIFU-induced cavitation. Engraving parameters: translational velocity 50 µm/s, 250 Hz PRF, 200 cycles, 20 passes, 33 MPa peak-positive-pressure amplitude.

intersection of lines. This can be attributed to the engraving procedure. Overlapping lines were engraved such that there was no spacing between them, i.e., line intersections received twice the sonication cycles compared to other locations. The poorly formed horizontal lines in the letter “A” can be attributed to the same mechanism; vertical lines were engraved first, likely serving as preferential bubble nucleation sites during engraving of the horizontal lines in close proximity.

From the surface topography maps micrometer-scale micropits and scratches were visible throughout the aluminium surface. This non-uniformity likely produced preferential bubble nucleation sites, potentially contributing to the non-uniformity of engraved lines. A more rigorous polishing method would improve surface uniformity, mitigating this effect. Alternatively, consistent surface roughness could facilitate cavitation uniformly. Using HIFU to initialize surface roughness before engraving calls for future research. Additionally, controlled and localized micrometer-scale surface roughening could be of interest in chemical processing, for instance for producing highly localized catalytic surfaces.

IV. Conclusions

This work demonstrates HIFU-induced surface erosion as a viable micrometer-scale machining technology. Control over line width and depth in engraving aluminium was achieved by varying sonication parameters. Compared to existing methods, HIFU-induced cavitation provides a unique combination of advantages: it is inexpensive, non-contact, performed in water immersion, and applicable to thermally sensitive materials.

References

[1] M. L. Crichton, C. Archer-Jones, S. Meliga, G. Edwards, D. Martin, H. Huang and M. A. Kendall, "Characterising the material properties at the interface between skin and a skin vaccination microprojection device," Acta Biomater., vol. 36, pp. 186-194, 2016.

[2] M. Vaezi, H. Seitz and S. Yang, "A review on 3D micro-additive manufacturing technologies," Int. J. Adv. Manuf. Technol., vol. 67, pp. 1721-1754, 2013.

[3] A. A. Bojang and H.-S. Wu, "Design, fundamental principles of fabrication and applications of microreactors," Processes, vol. 8, 2020.

[4] S. Gao and H. Huang, "Recent advances in micro- and nano-machining technologies," Front. Mech. Eng., vol. 12, no. 1, pp. 18-32, 2017.

[5] D. Ensminger and L. J. Bond, Ultrasonics: fundamentals, technologies, and applications, Boca Raton, Florida: CRC Press, 2011.

[6] S. Kalpakjian and S. Schmid, Manufacturing: engineering and technology, New Jersey: Pearson Prentice Hall, 2010.

[7] L. Wijngaarden, "Mechanics of collapsing bubbles," Ultrason. Sonochem., vol. 29, pp. 524-527, 2016.

[8] K. B. Bader, E. Vlaisavljevich and A. D. Maxwell, "For whom the bubble grows: physical principes of bubble dynamics in histotripsy ultrasound therapy," Ultrasound Med. Biol., vol. 45, no. 5, pp. 1056-1080, 2019.

[9] W. J. Tomlinson and S. J. Matthews, "Cavitation erosion of aluminium alloys," J. Mater. Sci., vol. 29, pp. 1101-1108, 1994.

[10] C.-T. Hsiao, A. Jayaprakash, A. Kapahi, J. Choi and G. L. Chahine, "Modelling of material pitting from cavitation bubble collapse," J. Fluid Mech., vol. 755, pp. 142-175, 2014.

[11] E. Skorb, D. Shchukin, H. Möhwald and D. Andreeva, "Ultrasound-driven design of metal surface nanofoams," Nanoscale, vol. 2, no. 5, pp. 722-727, 2010.

[12] S. Yoshizawa, T. Ikeda, A. Ito, R. Ota, S. Takagi and Y. Matsumoto, "High intensity focused ultrasound lithotripsy with cavitating microbubbles," Med. Biol. Eng. Comput., vol. 47, no. 8, pp. 851-860, 2009.

[13] Y. Zhou and X. Wang, "Effect of pulse duration and pulse repetition frequency of cavitation histotripsy on erosion at the surface of soft material," Ultrasonics, vol. 84, pp. 296-309, 2018.

[14] A. Jayaprakash, J.-K. Choi, G. L. Chahine, F. Martin, M. Donnelly, J.-P. Franc and A. Karimi, "Scaling study of cavitation pitting from cavitating jets and ultrasonic horns," Wear, vol. 296, pp. 619-629, 2012.

[15] A. Meriläinen, J. Hyvönen, A. Salmi and E. Hæggström, "CESAM-coded excitation scanning acoustic microscope," Rev. Sci. Instrum., vol. 92, no. 7, p. 074901, 2021.

[16] J. Hyvönen, A. Meriläinen, A. Salmi, L. Hupa, N. Lindfors and E. Hæggström, "Three Megapixel Ultrasonic Microscope Imaging," in IEEE Int. Ultra. Sym., Glasgow, 2019.

[17] R. C. Preston, Output measurements for medical ultrasound, London: Springer-Verlag, 1991.

[18] J. Yin, Y. Zhang, J. Zhu and L. Lv, "An experimental and numerical study on the dynamical behaviors of the rebound cavitation bubble near the solid wall," Int. J. Heat Mass Tran., vol. 177, no. 10, p. 121525, 2021.

[19] A. V. Pandit, V. P. Sarvothaman and V. V. Ranade, "Estimation of chemical and physical effects of cavitation by analysis of cavitating single bubble dynamics," Ultrason. Sonochem., vol. 77, p. 105677, 2021.